A Comparative Study on the Conductive Properties of Coated and Printed Silver Layers on a Paper Substrate

Cian Nash, Yann Spiesschaert, George Amarandei, Zlatka Stoeva, Rumen I. Tomov, Dan Tonchev, Isabel van Driessche & Bartlomiej Andrzej

Journal of Electronic Materials

ISSN 0361-5235

Journal of Elec Materi
DOI 10.1007/s11664-014-3434-5

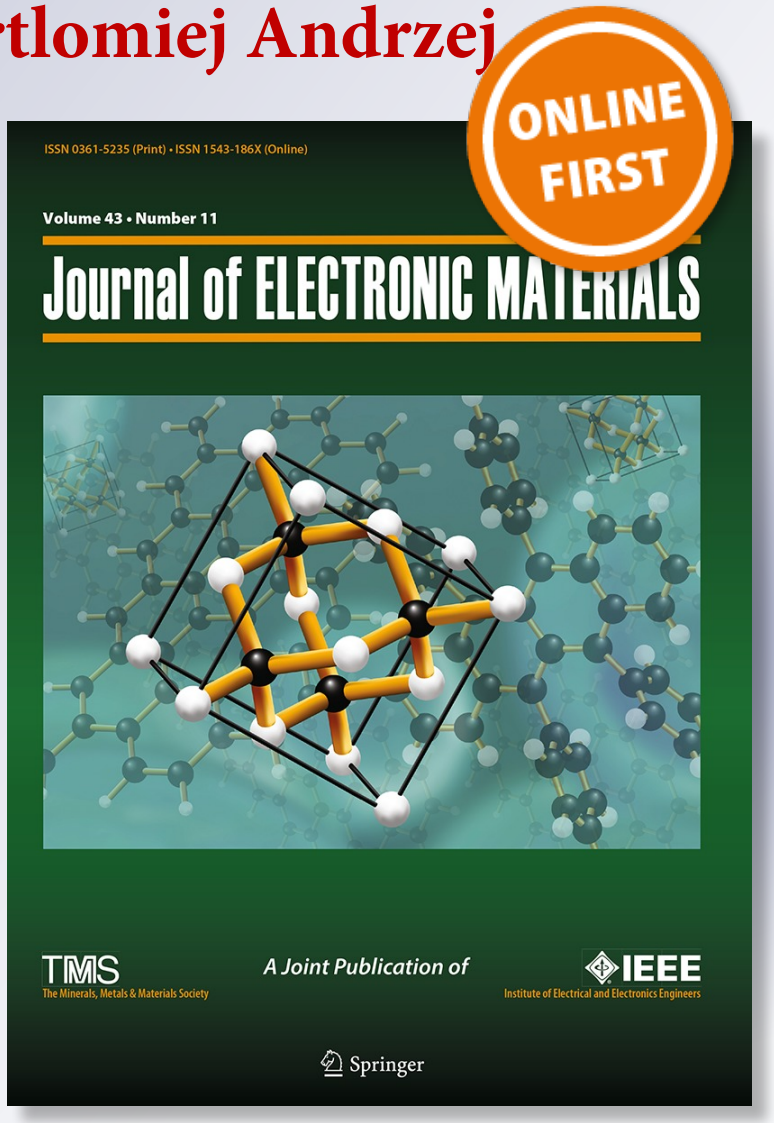

Springer

Journal of ELECTRONIC MATERIALS
DOI: 10.1007/s11664-014-3434-5

A Comparative Study on the Conductive Properties of Coated and Printed Silver Layers on a Paper Substrate

CIAN NASH,[1] YANN SPIESSCHAERT,[2] GEORGE AMARANDEI,[1,6] ZLATKA STOEVA,[3] RUMEN I. TOMOV,[4] DAN TONCHEV,[3] ISABEL VAN DRIESSCHE,[2] and BARTLOMIEJ ANDRZEJ GLOWACKI[1,4,5]

1.—Department of Physics and Energy, University of Limerick, Limerick, Ireland. 2.—Department of Inorganic and Physical Chemistry, Ghent University, Ghent, Belgium. 3.—DZP Technologies Ltd, Future Business Centre, Kings Hedges Rd, Cambridge CB4 2HY, UK. 4.—Department of Materials Science and Metallurgy, University of Cambridge, 27 Charles Babbage Road, Cambridge CB3 0FS, England, UK. 5.—Institute of Power Engineering (IEn), ul. Mory 8, 01-033 Warsaw, Poland. 6.—e-mail: george.amarandei@ul.ie

The industrial sector of flexible printed electronics has shown a dynamic growth in the last decades. Therefore, demand for new inks, coatings and printing methods leading to improved performances of the electronic components at room temperature is also increasing. Here, we present a study on the conductive properties of silver layers obtained by different coating and printing methods. The results obtained proved that drop-on-demand inkjet printing of water-based inks containing micron-sized silver flakes with narrow-size distribution is a feasible method for *in situ* fabrication of conductive silver coatings that does not require additional heat treatment. A rigorous optimization Taguchi experiment was carried out considering the major process parameters. This experiment showed that the printing pressure was the dominant factor defining the quality of the printed coatings and tracks.

Key words: Coating and printing technologies, inkjet printing, silver flake ink, conductivity, low temperature, Taguchi optimization

INTRODUCTION

For electronic components, the direct printing of metals from aqueous solutions or solvent-based inks is an important technique as it can produce continuous metallic pattern in a pre-defined manner on large variety of substrates.[1] Conductive inks find applications in the areas of printed and plastic electronics as conductive connectors in printed (rigid or flexible) circuit boards, flexible aerospace and automotive components, conductive grids for flexible displays screens, medical devices and bio-sensors, as well as energy-related components like electrodes in organic light-emitting diode applications, photovoltaics, current collectors in flexible batteries and supercapacitors printed on paper or nano-cellulose substrates.[2] These inks have to meet strict requirements in terms of performance and stability, processing temperatures, cost, energy efficiency, and ease of manufacture.

The metal precursor inks can be composed of either dissolved organometallic compounds and polymers or colloidal suspensions of metal micro- and/or nano-particles suspensions.[1] Over the years, a significant effort has been devoted to the production and utilization of silver particles of different morphologies (e.g., nanoparticles, nanowires, flakes, etc.) due to their high electrical conductivity, relatively high melting point, resistance to oxidation, excellent solder qualities, and reasonable price.[3] Therefore, silver conductive inks are used in plastic and printed electronics where electronic devices require multiple layers of conductive interconnects or electrodes.[1–3]

To obtain the desired patterns, the inks can be applied on a variety of substrates using different methods of coating (i.e. the ink layer is transferred

(Received March 27, 2014; accepted September 20, 2014)

Published online: 10 October 2014

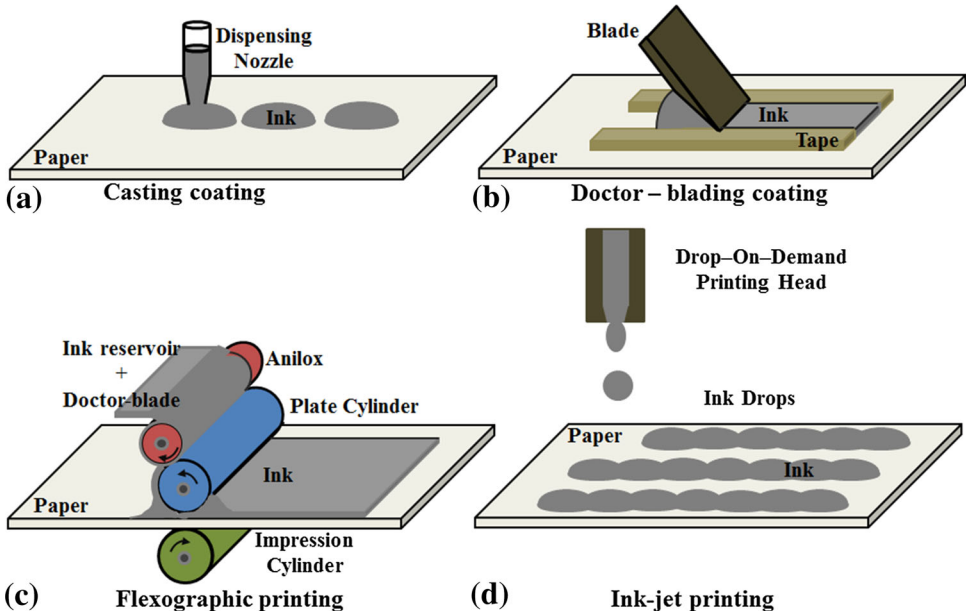

Fig. 1. Schematic representation of the different techniques used to create layers of conductive inks on paper substrate. (a) Casting—ink drops attached to the dispensing nozzle are brought into contact with the substrate and transferred due to capillary action. (b) Doctor-blading—an ink drop is placed on the substrate in front of a blade. By moving the blade small shear fields are applied and the substrate is coated. (c) Flexographic printing—the ink from a reservoir is transferred to the anilox and then to the plate cylinder (this can be flat or engraved). Then the ink is impregnated on the paper against the impression cylinder. The amount of ink at the contact point between the plate cylinder and the paper is exaggerated for illustration purpose. (d) Ink-jet printing—in drop-on-demand (DOD) the ink is released in small quantities from a nozzle at high speeds. The drops impact with the substrate and/or with the previous deposited droplets leading to the desired coating thickness.

to the substrate by pouring, spraying, casting or smearing it over the surface) or printing (by which the layer of ink is transferred from a stamp to a substrate by a reversing action).[4] Coating techniques include spin, spray, curtain, casting, painting, knife-over-edge coating, doctor blading, etc., while printing techniques can be screen, pad, gravure or flexographic. Ink-jet printing is a standalone technique that could be placed in both categories as it can apply uniform coatings but also offers the possibility to reproduce a complex pattern in a one-step process.[4] In the areas of flexible and paper electronics, coating and printing techniques can be used either individually or combined in order to reduce the number of processing steps.

In this study, we compare the effect of four deposition techniques, i.e. casting, doctor-blading, flexographic and ink-jet printing, on the electric conductivity of the deposited tracks.

Casting (Fig. 1a) is the simplest experimental technique that can be employed for substrates coating.[4] No sophisticated equipment is needed but a good horizontality of the substrate surface is essential. The ink is simply cast onto the substrate in the form of isolated drops or liquid portion and then dried at room or elevated temperature. This simple procedure allows for thick films with good quality of the coating to be obtained, but it lacks the precision of the film thickness control. Also, the wetting properties of the inks are important as dewetting can occur during drying leading to inhomogeneous coatings.[4]

Doctor-blading (Fig. 1b) allows for the formation of films with a well-predefined thickness ranging from 10 μm to 500 μm while the ink loss during coating can be minimized to less than 5 (wt.%).[4,5] This technique uses a sharp blade placed at a fixed distance above the surface of the substrate and it can be applied for both grooved and flat surfaces. The ink is placed in front of the blade that is then moved linearly across the substrate. The thickness value of the coated layer depends on the meniscus between the blade and the wet film on the trailing edge of the blade as this is related to shear field (proportional to the speed of the blade). Other factors that can influence the film thickness are the surface energy of the substrate and/or its porosity, and also the surface tension and the viscosity of the ink. The final dry thickness of the film will be proportional to the gap width and the concentration of the solid material present in the solution.[4] The linear speed during the doctor-blading can vary between 1 mm s^{-1} and 100 mm s^{-1}, which leads to relatively small shear stress applied during coating.[4,5] An alternative to this technique is represented by *bar-coating* that has a similar working principle, but in this case a bar rolls the ink over the substrate.[2,6]

Flexographic printing (Fig. 1c) has been demonstrated to be a reliable technique for organic

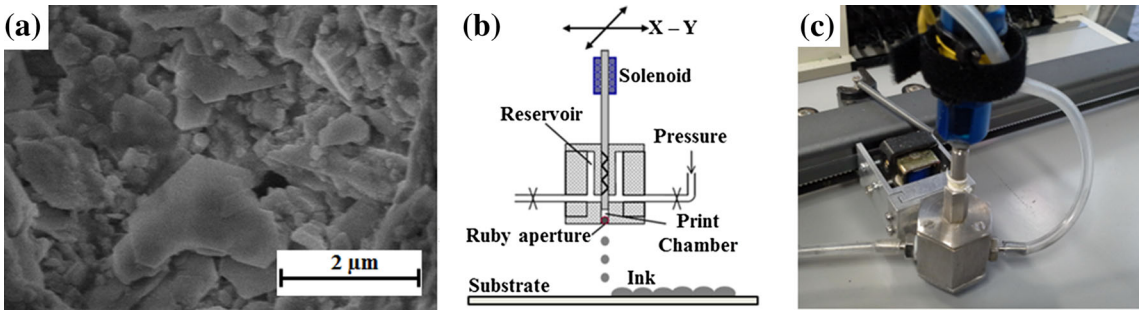

Fig. 2. (a) The SEM image of coated proofing paper revealing the microstructure of the paper. (b) Schematic diagram and (c) optical image of the DOD ink-jet printing head used in this study. The printing head was attached to a Roland plotter DXY 1150 to allow for X–Y movement with a step resolution of 25 μm.

electronics, and photovoltaic and battery applications.[7] Its working principle is based on the transfer of the desired image using relief plates that impose a low pressure onto the substrate.[7,8] During the printing procedure, the ink is transferred from a reservoir to an anilox (micro-engraved cylinder) by a doctor blade and then onto a printing plate. The anilox micro-cells are always filled with a constant ink volume. The printing plate defines the pattern information. While the inked pattern is pressed between the printing plate and printing cylinder against the substrate, the ink transfer is made by ink film scission. When a solid pattern is printed, its thickness depends on the ink volume in the anilox cells, on the ink-substrate affinity, and on the number of ink layers.[7] The roller pressure during flexographic printing is typically around 100 Pa, and will depend on parameters such as the nature of the roller material that will influence its hardness, the impression distance, the substrate material, the printing speed (e.g., for a hand flexo-proofer this is $\sim$0.1 m s^{-1}).

Ink-jet printing (Fig. 1d) is a relatively new technique used in energy and electronics industrial applications.[4] In the drop-on-demand mode (DOD), ink-jet printing has the advantage of delivering controlled small amounts of ink onto the substrate creating the desired pattern with minimal ink waste,[9,10] and with minimal influence on and without direct contact with the substrate.[11] Nowadays, the majority of commercial inkjet printers are based on DOD technology utilizing thermal, piezoelectric, electrostatic or acoustic methods of droplet generation.[12] Alternatively, the electromagnetically actuated print head (see Fig. 2) can be used as a DOD method in order to minimize ink heating and to reduce the procedure complexity.[13] The nozzle aperture can be machined to the desired tolerance whilst exhibiting resistance to wear and corrosion, but its size is fixed. A constant pressure is provided by an external air compressor allowing the production of drops as a solenoid driven plunger opens and closes the nozzle orifice. The drop size can be controlled by varying the opening time and/or the rheological properties of the ink. The method allows for the movement of either the nozzle or the substrate. Thus, the relative positions of the print head and substrate may be adjusted accurately and rapidly by using a computer-controlled X–Y stage.

It can be anticipated that, if one particular ink composition is used, the methods presented in Fig. 1 will lead to different properties of the coatings deposited onto the substrates as the ink kinetics is method-dependent. Therefore, finding the differences that can occur, and determining the technique that can deliver, a particular set of specifications (e.g., target conductivity, film thickness, etc.) for a particular ink composition is important as this will influence the success and the efficiency of chosen deposition method. Moreover, all the methods presented in this paper are used in day-to-day industrial applications, therefore optimizing the technique that delivers the required quality of the ink layer is important from technological perspectives.

In the present paper, we investigated the effect of the coating and printing methods presented above on the microstructure and conductivity of the resulting silver layers formed on paper substrates. In the experiment, we used a specially formulated water-based ink with silver micron-sized flakes of narrow-size distribution in an attempt to determine the optimum silver printing process for paper electronics. Commonly used silver nanoparticles-based inks are not suitable for this application because they typically require high temperature treatment to sinter the nanoparticles, and use solvents that can deform or degrade the paper substrates.

We show that, for this particular ink composition, only the ink-jet printed coatings revealed high conductivity after deposition at room temperature with no further sintering process being required. Using a Taguchi optimization method, the influence of the different process parameters, like ink thinning, pressure, opening time and drop density, on the conductivity of the ink-jet printed layers were evaluated and discussed.

EXPERIMENTAL

Materials

An aqueous-based silver ink formulated by DZP Technologies, UK, was used for the coating and printing experiments. The silver content of D38NV ink was 52 (wt.%) and the ink viscosity was 10 Pa s. The silver flakes had a narrow size distribution with 10% < 1.1 μm, 50% < 2.1 μm and 90% < 3.9 μm. For some of the printing experiments, the ink was thinned with deionized water (18 MΩ cm) in the desired ratios (as presented later in the paper). Rigorous shaking and stirring was performed before the deposition procedure in order to achieve a homogenous mixture. In all coating and printing experiments, KPP/SHC proofing paper sheet from RK Print Coat Instruments, UK, with a Brunauer–Emmett–Teller (BET) surface area of 23.5 $m^2\ g^{-1}$, was used as substrate. The scanning electron microscopy (SEM) image of this substrate is presented in Fig. 2a. Thus, the effect of the ink–substrate interactions (e.g., substrate wettability, porosity) was maintained constant and, therefore, not discussed in this paper. Thus, the final results will be influenced only by the method used to deliver the ink onto the substrate.

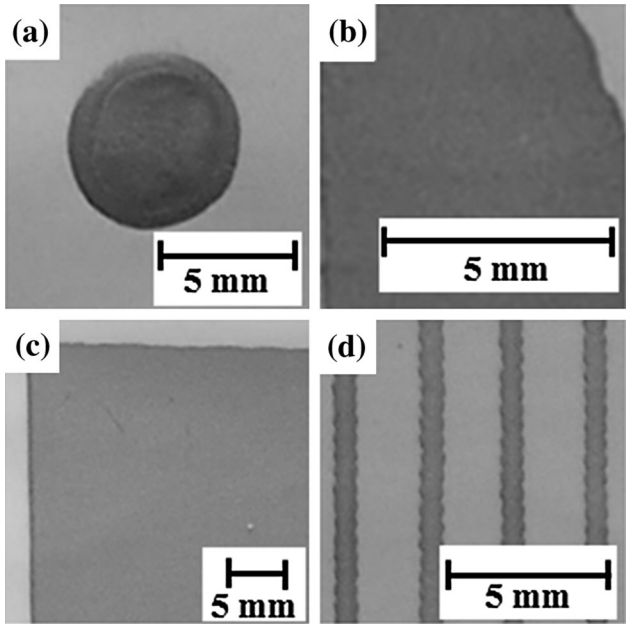

Fig. 3. Optical images of (a) a typical ink-drop deposit by *casting*; (b) a layer coated using doctor-blading; the speed of the blade was kept at ≈0.01 m s^{-1}; (c) a typical flexographic printed layer; the printing speed was 0.1 m s^{-1}. (d) typical silver tracks obtained using DOD ink-jet printing; the drop speed varied with the printing parameters but the typical values were 1–2 m s^{-1}.

Coating and Printing Methods Implementation

The *casting* coating method used consisted of applying a fixed amount (~100 μL) of as-received or thinned ink onto the paper substrate. The distance between the dispensing nozzle and the substrate was minimized until the ink drop was deposited mainly due to capillary action. The liquid deposition led to drops of 4–7 mm diameter (Fig. 3a). The coated surface was then dried at room temperature. However, even after few days, the core of the coated layers remained wet.

In the *doctor-blading* procedure, ink drops with similar sizes as for casting were used. The drops were placed between two tape tracks. This simple configuration allowed for a constant gap between the blade and the substrate during coating. A sharp laboratory blade was then moved across the substrate at a constant speed of approximately 0.01 m s^{-1}. The procedure was then repeated for the *bar coating* method, thus mimicking the bar methods described in Refs. 2 and 6. In the present case, a cylinder with a non-porous rubber shell and metal inner core was used. A spongious material was present between the rubber shell and the metal core. This method led to similar results as *doctor-blading*.

For *flexographic printing*, only as-received ink was used. The printing was performed at a speed of 0.1 m s^{-1} leading to smooth layers, as seen in Fig. 3c. The films were printed using a hand flexographic proofer with 200 lpi and a Q type cell (quad anilox engraving) with a volume of 9.0 bcm. In a control experiment, the same flexographic printing arrangement was used to print silver films using a commercial flexographic ink containing silver powders of wide-size particle distribution (ink F50NV formulated by DZP Technologies) and this led to a fully conductive film, no sintering process being required (data not shown).

Ink-jet printing was performed using thinned ink as the as-received ink was too viscous for direct use in the ink-jet printing head. The print chamber (Fig. 2b and c) was emptied and cleaned by purging with water and isopropyl alcohol before a fresh ink was used.

The electromagnetically actuated ink-jet system was controlled by hardware (Macrojet X–Y controller) and software developed within the TEMPRI project.[14] This allows for the printing of custom raster scan patterns. The nozzle aperture was defined by a ruby orifice of 100 μm in diameter (Fig. 2b). The jetting pressure was provided by means of compressed air controlled by a high precision adjustable regulator (SMC IR3000-04). The print nozzle was moved over the substrate by a Rolland X–Y plotter with a step resolution of 25 μm. For all ink-jet experiments presented in this paper the printing speed and the inter-drop wait time were maintained constant, at 100 mm s^{-1} and 250 μs, respectively.

Conductivity Measurements

The patterns resistance was measured using a Jandel 4 point probe with a Matt TC tip (radius ~100 μm, probe spacing ~1 mm). The probes were placed on each of the lines, the current between the outer pins was set to I = 100 mA, and the voltage V across the inner pins was measured. Five values were measured for each pattern. The resistance (R) per unit length (l) was calculated using $\frac{R}{l} = \frac{V}{I}$. The resistivity ρ was calculated by multiplying the resistance per unit length by the cross-sectional area A (as determined from the SEM images). The obtained resistivity values were then used to evaluate the conductivity σ of the layer since $\sigma = \frac{1}{\rho}$. The conductivity values were then employed to determine the signal-to-noise (S/N) ratios and the average conductivity for each trial in the Taguchi analysis as described in "The Taguchi Optimization Method" section. When no conductivity was measured (i.e. no voltage across the inner pins was present), the zero values were assigned.

In all cases, the ink layers and tracks were used "as printed" without any thermal or other type of post-treatment or sintering.

Image Analysis

The microstructure of the ink layers was inspected by scanning electron microscopy (SEM) using a Hitachi S4800 FESEM operating at 5 kV. Images analysis was performed using the open-source image processing package FIJI, which is based on ImageJ (National Institutes of Health, USA). Low magnification top-view SEM images gave information on the quality of ink-jet printed layers surface. At larger magnification, the shape and the 2D projected area of the silver flakes could be determined. Using this information, the surface coverage (defined as being the total 2D projected area of silver divided by the total area of the image) was evaluated. However, the surface coverage would reflect only the flakes visibility as these were found to be oriented predominantly in a horizontal plane, but in some cases they tended to have a 3D orientation. The SEM investigation of the layer cross-section allowed estimating the relative amount of silver present in the layers as represented by the filling ratio (defined in a similar manner as coverage) and also to observe the flakes vertical distribution and their connectivity. The layers thickness was also estimated from the SEM cross-sections.

RESULTS AND DISCUSSION

Casting the silver ink onto the paper substrate led to the formation of uniform and relatively thick layers (Fig. 3a) with thicknesses of ~200 μm or larger. The layers exhibited an inner wet structure present after days of drying at room temperature as a result of the substantial thickness that prevented water removal in the absence of further thermal treatment. For *doctor-blading*, similar drops were first cast on the substrate and then bladed. This led to uniform coatings (Fig. 3b) of silver ink on the paper. The *doctor-blading* experiments were performed for as-received and thinned (in a ratio of 40% ink and 60% water) inks, resulting into coatings with thicknesses of 27 μm and 38 μm, respectively. *Flexographic printing* of the as-received ink led to a film thickness of 7 μm while the *ink-jet* printing of the thinned ink (40% ink and 60% water) produced tracks approximately 19 μm thick.

Conductivity measurements were performed on all the layers. Only the tracks obtained by ink-jet printing the thinned ink were conductive. No conductivity values were obtained for the 4-point probe measurements of the other samples.

As different techniques were used, it was expected that the difference in the conductivity of the silver layers would be related to the inner morphology as an effect of the silver flakes connectivity and the formation of conductive percolating paths.

Microstructure

Both *doctor-blading coating* (Fig. 4a) and *flexographic printing* (Fig. 4b) were revealed to produce uniform distribution of the flakes within the layer when as-received ink was used. The flakes visual distribution does not seem to differ significantly when the water-thinned ink is coated by doctor-blading (Fig. 4c). Therefore, in these samples, a significant number of brighter regions (due to overcharging with the electron beam) containing the residual polymer carrier (RC) can be observed in the SEM images (Fig. 4a and b). These RC regions kept the flakes apart. Therefore, the flakes could not form a conductive path. For the layer obtained by ink-jet printing, however, the top-view SEM images (Fig. 4d) were dominated by the silver flakes presence forming a continuous network.

The cross-sections of the layers (Fig. 5) showed similar distribution of the flakes within the layers. Thus, after *blading* (Fig. 5a and c) and *flexographic printing* (Fig. 5b), the silver flakes remain isolated by the RC while after ink-jet printing the flakes are oriented in-plane and compacted (Fig. 5d).

The SEM analysis of the layers (Figs. 4a–c, 5a–c) suggested that the silver flakes were randomly distributed within the layer and separated by large areas of residual carrier regions, but the flakes are connected locally leading to small isolated clusters or nests (see Fig. 5). These nests were far apart and no percolating path that could allow for the electrical conductivity occurrence was formed.

Electrical Conductivity

The electrical conductivity data measured (Fig. 6) were analyzed in relation with the flakes surface coverage from the top view images (Fig. 4) and the

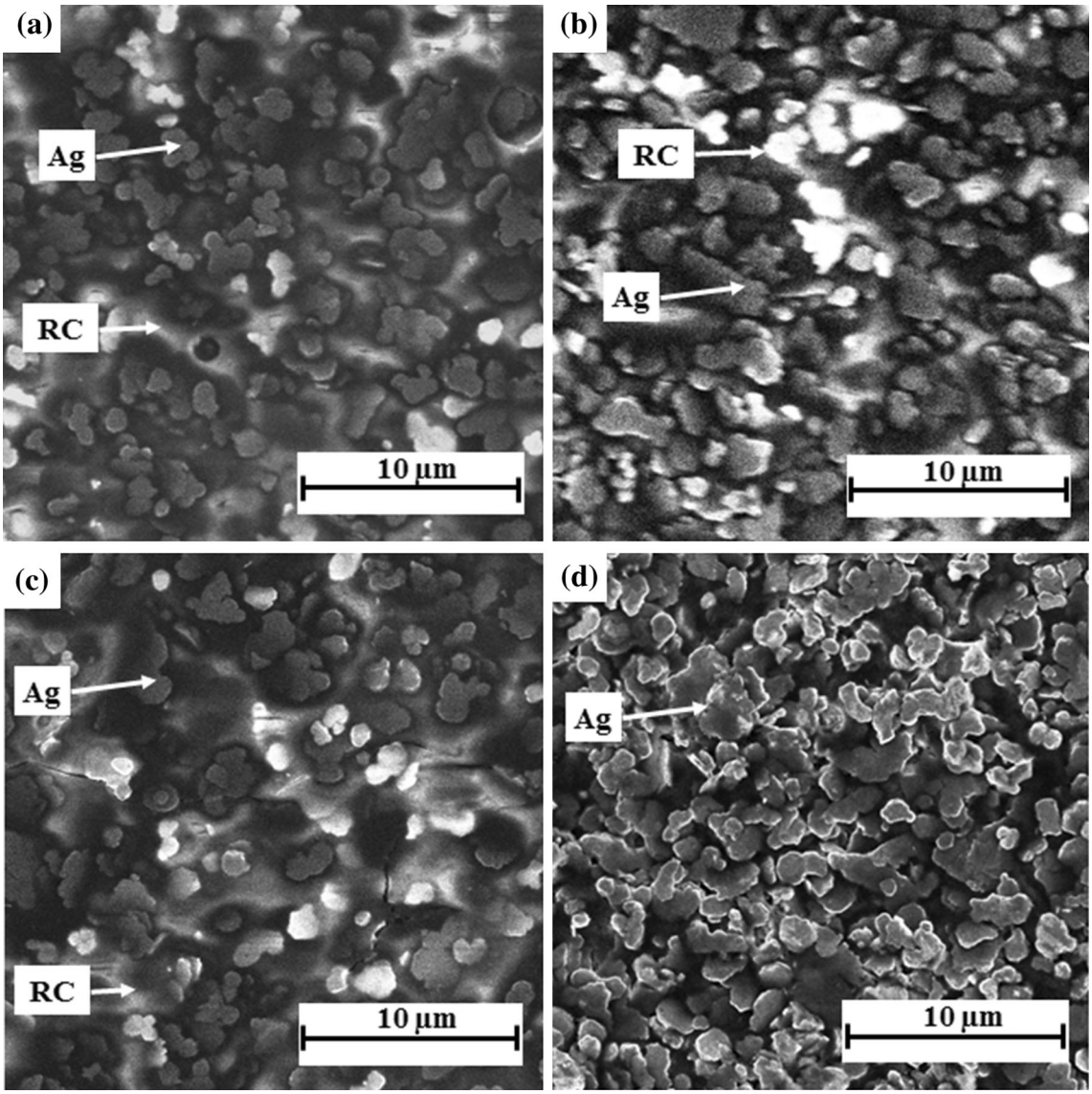

Fig. 4. Top-view SEM images of the silver ink (D38NV) layers using: (a) doctor blading of the as-received ink; (b) flexography of the as-received ink; (c) doctor blading of a thinned ink (40% ink and 60% water); (d) inkjet printing of a thinned ink (40% ink and 60% water). The printing parameters were opening time τ = 275 μs, jetting pressure P_j = 0.6 bar, drop density ρ_d = 2 drops mm^{-1}. The presence of the residual polymer carrier (*RC*) and of the silver (*Ag*) flakes is indicated by arrows.

filling ratio from the cross-section images (Fig. 5). It can be observed (Fig. 6) that, for small coverage and filling ratios (corresponding to isolated nests flakes), the conductivity was zero, while for enhanced flake compaction (as reflected by the larger coverage and filling ratios) the layers became electrically conductive. Only the ink-jet printed coatings were found to be conductive. The samples coated using doctor-blading (i.e. samples a and c) have similar coverage and filing ratio independently of their thinning. This suggests that the ink-thinning might play a secondary role in the final morphology.

Although the thinnest layers were obtained by flexographic printing, the highest compaction of the flakes was observed for ink-jet printing. The thinned ink was utilized in ink-jet printing and doctor-blading experiments. In the latter case, no significant difference in the flakes distribution within the layer was observed when compared with as-received ink experiments (compare Fig. 4a and c with Fig. 5a and c, respectively). This observation suggested that the changes in the conductivity should be related not to the variation of the ink mass load percentage but to the silver flakes kinetics during the coating or printing processes.

Ink Flow Dynamics and its Possible Influences on Conductive Properties of the Layers

The ink dynamics and ink transfer inherent to the different coating and printing methods are complex processes that depend on ink properties, e.g., viscosity

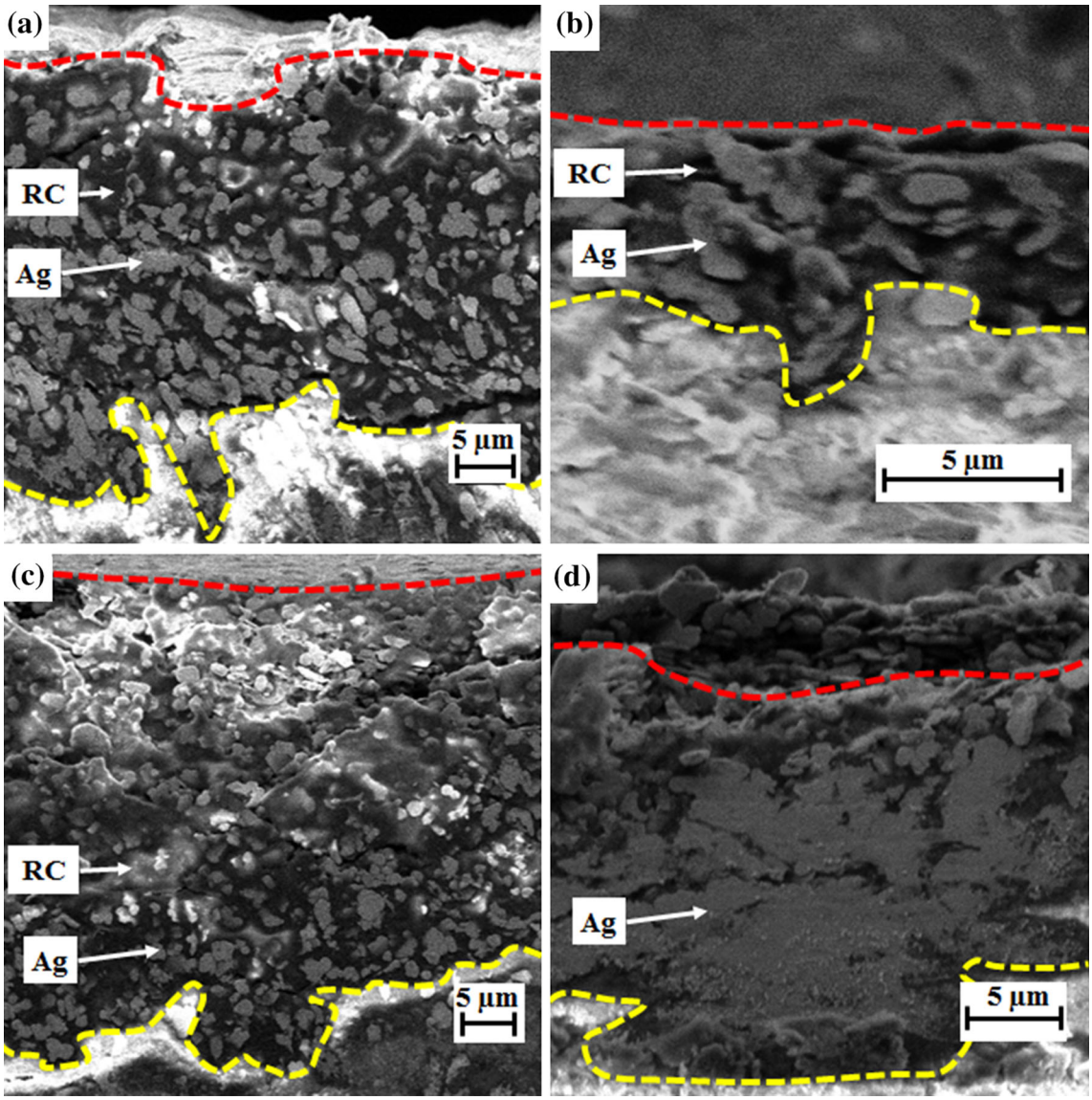

Fig. 5. Cross-section SEM images of the silver ink (D38NV) layers using: (a) doctor blading of the as-received ink; (b) flexography of the as-received ink; (c) doctor blading of a thinned ink (40% ink and 60% water); (d) inkjet printing of a thinned ink (40% ink and 60% water). The printing parameters were opening time τ = 275 μs, P_j = 0.6 bar, ρ_d = 2 drops mm^{-1}. The presence of the residual polymer carrier (*RC*) and of the silver (*Ag*) flakes is indicated by arrows. The dotted lines show layers with a thickness of (a) 27 μm, (b) 7 μm, (c) 38 μm and (d) 19 μm, respectively.

and surface tension (both parameters also being directly related to the solid content of the ink), on the paper properties (roughness or porosity) and on the paper–ink interactions. Due to the complexity of the processes involved, it is not a trivial task to determine the individual influence of each parameter as, most of the time, they are interrelated. Here, for all methods the same ink (or its thinned variants) and the same paper substrate were used, the importance of these factors becomes secondary to the influence exerted by the coating and printing methods. Significant efforts have been made in the last decades to model the different type of ink flows, and it is beyond the scope of this paper to give a complete fluid dynamics description of the ink-flow for the different methods employed. Therefore, in this paper, we will limit the discussions just to the description of the main kinetic factors that could lead to the observed changes in the conductivity of the silver layers.

The paper–ink interaction depends on the coating and printing method used. Nevertheless, this interaction could be divided into three common stages. In the first stage, the ink makes contact with the substrate and the liquid carrier starts to be absorbed by the paper. In the second stage, the flakes tend to agglomerate and a partially dried film forms. As the flakes aggregate, they also start to reach the paper and block the pores. Consequently, the residual liquid carrier will be trapped within the deposited layer. In the third stage, a consolidation of the dried film occurs. At this stage, the liquid carrier

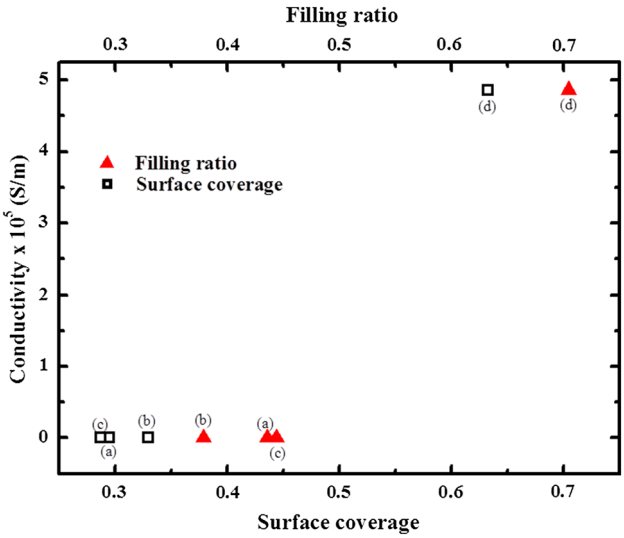

Fig. 6. The conductivity of the different layers as function of the filling ratio and surface coverage corresponding to the samples described by the SEM images from Figs. 4 and 5.

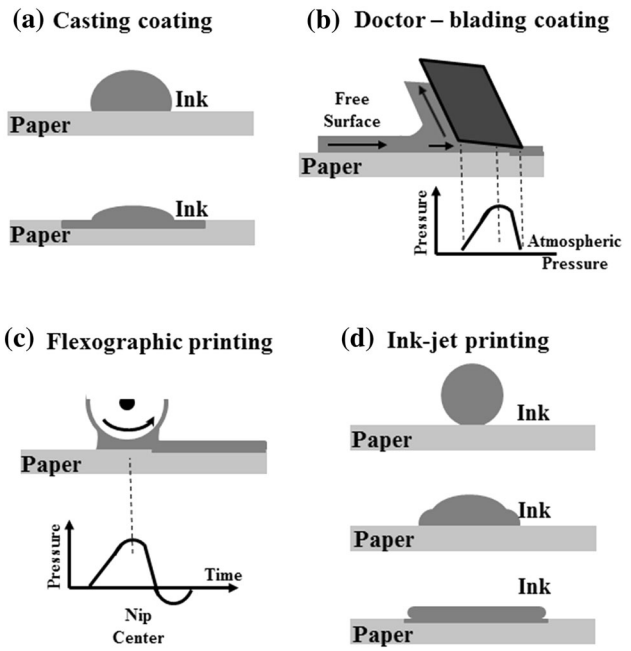

Fig. 7. Schematic representation for flow and pressure profile during the different methods used for coating and printing. (a) Casting coating—the ink flow is dominated by the capillary forces as the external pressure $P_e = 0$; (b) Doctor-blading coating—the ink flow and pressure profile during blading; the arrows indicate the typical mass flow lines during the coating;[18–20] (c) Flexographic printing—the printing nip and the pressure pulse; the arrow indicates the rotation direction of the nip during printing;[17] (d) Ink-jet printing—the droplet shape and diameter changes during the impact with the substrate.[22] For all schematics, the ink absorption into the paper substrate is represented for illustration purpose only.

loss can happen only through evaporation as the permeation through the paper pores is obstructed. The in-plane motion of particles is expected to be small under typical drying conditions, while the motion of the particles into the paper pores is prevented by a bridging mechanism.[15,16] For inks with a relative high initial volume fraction flakes (as that used in this study with the exception of thinned ink-jet ink variants), the pores can be blocked by a group of particles trying to enter the pore simultaneously. Usually the pores are blocked almost immediately. This blocking mechanism provides an explanation for the wet core of the casted layers persisting days after coating as well as for the presence of the RC in the layers deposited by doctor-blading or flexographic printing. The duration of each stage will depend on the ink properties, e.g., the initial solid volume of the ink, and also on the capillary-driven process taking place during the coating and printing.

A simple Bosanquet model can be applied for studying this capillary-driven process.[17] Thus, provided that the Poisseuille's law applies, the effects of the force due to momentum exchange of ink fluid in a capillary tube and the circumstances under which these effects become negligible can be investigated. In its mathematical form, the Bosanquet model can be written as:

$$\frac{\mathrm{d}}{\mathrm{d}t}\left(\pi R_c^2 \rho_m x \frac{\mathrm{d}x}{\mathrm{d}t}\right) + 8\pi\eta x \frac{\mathrm{d}x}{\mathrm{d}t} = P_e \pi R_c^2 + 2\pi R_c \gamma \cos\theta, \quad (1)$$

where R_c is the capillary tube radius, ρ_m is the mass density, x the length of the fluid column, η the viscosity of the liquid, γ the liquid surface tension, and θ the contact angle. The first term on the left-hand side accounts for the force due to the momentum exchange of the liquid in a capillary tube (here represented by the paper pore), and the second term is the viscosity drag of the liquid. On the right-hand side, the first term corresponds to the external pressure P_e while the second term corresponds to the capillary force. Thus, it can be observed that a significant increase in the external pressure can determine the capillary forces to become inappreciable.

In the *casting* procedure, no external pressure is applied ($P_e = 0$) and, therefore, the entire flow is driven only by the capillary forces (Fig. 7a). Therefore, compaction of the flakes is minimal and the thick layers deposited are not conductive. Moreover, the liquid carrier is not fully absorbed as the pores will be blocked by the flake nests, maintaining the inner core of the coating wet after long periods of time.

During *doctor-blading*, the liquid flows in the gap between the blade and the substrate (Fig. 7b). As liquid is dragged by the wedge, an adverse pressure gradient is formed, which opposes the drag flow. Therefore, the blade removes the excess of coating and acts as self-metering smoothing system.[18] The pressure distribution under the blade was found to be strongly dependent on the blade operating angle,

and whether or not the blade is stiff or whether the blade erosion takes place.[18,19] As the coating speed used was small (~0.01 m s^{-1}), the expected values for the pressure would be small. When blading is applied to liquid dispersions containing particles such as the present ink, structures of the particles can form in the shear fields. The size of these structures varies with the shear fields, and they can even span the gap between the paper and the blade.[21] However, these large bridging structures were not observed, confirming the existence of small shear fields.

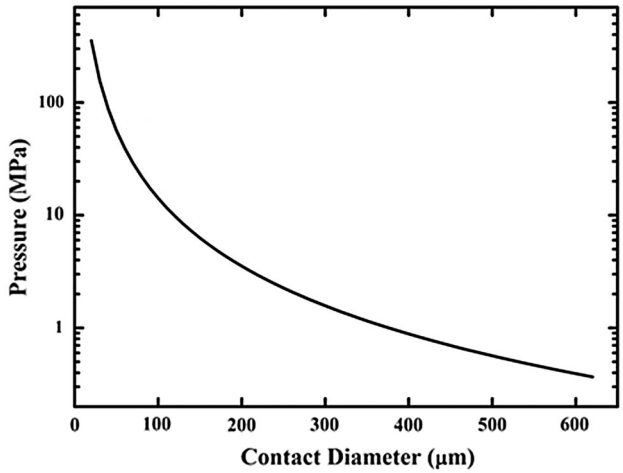

Fig. 8. The impact pressure decreases as the droplet reaches the maximum spreading and its final diameter.

In *flexographic printing*, the external pressure P_e is due to the printing nip and it varies with the pulse, vanishing when the pulse finishes.[17] In the present paper, a hand flexographic proofer was used where no impression cylinder is present. The roller pressure during the flexographic printing is typically below 100 Pa, and will depend on a range of parameters such as the nature of the roller material, the impression distance, the substrate material, the printing speed, etc. The dynamic nip pressure (see Fig. 7c) used in the present case is estimated to be about 0.1–0.2 MPa. This larger pressure can then account for the thinner films seen after flexographic printing. The pressure profile (Fig. 7b) for the blading[20] is similar to that for the flexographic printing (see Fig. 7c) leading to similar morphologies (compare Fig. 4a and b).

In *ink-jet printing*, after the contact with the substrate, the drop starts to spread as the inertia of the droplet causes a forced wetting. Upon contact with the substrate, the droplet starts to deform and the liquid is pushed radially outwards from the initial contact point. During spreading, the velocity normal to the surface will decrease from the initial impact velocity to zero as spreading finishes. This velocity reduction can lead to changes in droplet dynamics which is governed by the balance between the surface energy, the viscous dissipation and the inertia.[22]

The impact pressure of the inkjet droplets can be determined using the mass, the initial velocity and contact diameter of the droplet. The mass, the diameter and the velocity of droplet can be estimated from previous drop-watcher experiments,[10,13,23,24] while the diameter of the droplet

Table I. Chosen factors and levels for the ink-jet printing experiments

Level	Water/ink ratio (v/v) Factor A	Pressure (bar) Factor B	Opening time (μs) Factor C	Drop density (drops/mm) Factor D
1	0.4	0.45	255	2
2	0.5	0.5	275	2.2
3	0.6	0.6	300	2.5

Table II. $L_9(3^4)$ orthogonal array (9 runs and 4 factors)

	Levels			
Exercise	Factor A	Factor B	Factor C	Factor D
1	1	1	1	1
2	1	2	2	2
3	1	3	3	3
4	2	1	2	3
5	2	2	3	1
6	2	3	1	2
7	3	1	3	2
8	3	2	1	3
9	3	3	2	1

Table III. Taguchi inner arrays of: (a) conductivity; (b) filling ratio; (c) surface coverage; and (d) layer thickness

(a) Conductivity

Exercise	Water/ink ratio (v/v) Factor A	Pressure (bar) Factor B	Opening time (μs) Factor C	Drop density (drop/mm) Factor D	Conductivity (S/m) $\times 10^5$	*S/N* ratio
1	0.4	0.45	255	2	0.00041	45.80
2	0.4	0.5	275	2.2	1.38	116.86
3	0.4	0.6	300	2.5	2.25	121.15
4	0.5	0.45	275	2.5	1.91	119.83
5	0.5	0.5	300	2	2.09	117.66
6	0.5	0.6	255	2.2	1.53	114.70
7	0.6	0.45	300	2.2	0.046	87.48
8	0.6	0.5	255	2.5	2.47	121.91
9	0.6	0.6	275	2	4.86	127.75

(b) Filling ratio

Exercise	Water/ink ratio (v/v) Factor A	Pressure (bar) Factor B	Opening time (μs) Factor C	Drop density (drop/mm) Factor D	Filling ratio	*S/N* ratio
1	0.4	0.45	255	2	0.46	−6.82
2	0.4	0.5	275	2.2	0.76	−2.35
3	0.4	0.6	300	2.5	0.70	−3.09
4	0.5	0.45	275	2.5	0.65	−3.78
5	0.5	0.5	300	2	0.71	−3.03
6	0.5	0.6	255	2.2	0.67	−3.45
7	0.6	0.45	300	2.2	0.64	−3.94
8	0.6	0.5	255	2.5	0.58	−4.81
9	0.6	0.6	275	2	0.71	−3.04

(c) Surface coverage

Exercise	Water/ink ratio (v/v) Factor A	Pressure (bar) Factor B	Opening time (μs) Factor C	Drop density (drop/mm) Factor D	Surface coverage	*S/N* ratio
1	0.4	0.45	255	2	0.38	−8.43
2	0.4	0.5	275	2.2	0.45	−6.94
3	0.4	0.6	300	2.5	0.49	−6.09
4	0.5	0.45	275	2.5	0.51	−5.82
5	0.5	0.5	300	2	0.72	−2.81
6	0.5	0.6	255	2.2	0.83	−1.57
7	0.6	0.45	300	2.2	0.88	−1.12
8	0.6	0.5	255	2.5	0.85	−1.42
9	0.6	0.6	275	2	0.63	−3.97

(d) Layer thickness

Exercise	Water/ink ratio (v/v) Factor A	Pressure (bar) Factor B	Opening time (μs) Factor C	Drop density (drop/mm) Factor D	Thickness (μm)	*S/N* ratio
1	0.4	0.45	255	2	31.4	90.01
2	0.4	0.5	275	2.2	42.8	87.37
3	0.4	0.6	300	2.5	35.5	89.00
4	0.5	0.45	275	2.5	24.5	92.17
5	0.5	0.5	300	2	24.9	90.92
6	0.5	0.6	255	2.2	28.9	90.71
7	0.6	0.45	300	2.2	30.1	90.42
8	0.6	0.5	255	2.5	24.2	92.27
9	0.6	0.6	275	2	19.7	93.99

Table IV. Taguchi response tables of the (a) conductivity (LB); (b) filling ratio (LB); (c) surface coverage (LB); and (d) layer thickness (SB)

Level	Water/ink ratio	Pressure	Opening time	Drop density
(a) Conductivity				
1 (low)	94.60	84.37	96.08	97.07
2 (medium)	117.40	118.81	121.48	106.35
3 (high)	112.38	121.20	108.76	120.96
S/N variation (maximum–minimum)	22.80	36.83	25.40	23.89
Ranking	4	1	2	3
(b) Filling ratio				
1 (low)	−4.09	−4.85	−4.44	−4.30
2 (medium)	−3.42	−3.40	−3.06	−3.25
3 (high)	−3.93	−3.19	−3.35	−3.89
S/N variation (maximum–minimum)	0.66	1.65	1.38	1.05
Ranking	4	1	2	3
(c) Surface coverage				
1 (low)	−7.15	−5.12	−4.66	−5.07
2 (medium)	−3.40	−3.72	−5.58	−3.21
3 (high)	−2.17	−3.88	−3.34	−4.44
S/N variation (maximum–minimum)	4.98	1.40	2.24	1.86
Ranking	1	4	2	3
(d) Layer thickness				
1 (low)	88.80	90.87	91.57	91.64
2 (medium)	91.26	90.19	91.18	89.50
3 (high)	92.23	91.24	90.11	91.15
S/N variation (maximum–minimum)	3.43	1.05	1.46	2.14
Ranking	1	4	3	2

relics can be measured from optical micrographs. This implies that the ink droplet has a mass m of ~6 μg, an initial velocity U_0 = 1 m s^{-1} and contact diameter D impacting with a rigid substrate. The initial droplet diameter D_0 = 200 μm represents the diameter of the droplet in flight. The final diameter of the droplet after impact with the substrate D_f is measured to be approximately 600 μm with a film thickness of 20 μm. The pressure is then estimated by assuming that the deceleration of the droplet on impact (as reflected by the changes in the droplet acceleration a) is the deceleration required to stop the topmost portion of the droplet as it collapses to the final film thickness of 20 μm. Assuming a circular contact area with diameter D, the pressure is given by $P = \frac{F}{A}$ which in this case becomes $P = \frac{4ma}{\pi D^2}$. The pressure varies (Fig. 8) from 300 MPa at a contact diameter of 20 μm to 0.3 MPa at a contact diameter of 600 μm, i.e. the final droplet diameter.

The estimated impact pressures representing the external pressure term P_e are shown in Fig. 8. It is obvious that, during the most of the drop-spreading time, the pressures are significantly higher than the ones applied for any of the other techniques. Thus, we can speculate that ink-jet printing of the as-described silver ink leads to highest compaction of the silver flakes (see Fig. 5). Thus, the significant shear forces experienced by the elongated flakes tend to their in-plane orientation and to compact them. The result is the appearance of percolation paths consisting of silver-flakes nests and, consequently, the increase in the conductivity without any additional sintering.

The Taguchi Optimization Method

To understand the influence of the process parameters on the formation of conductive layers when using inkjet printing, an optimization by the Taguchi method was performed. The ability of the Taguchi technique to determine the optimal parameters to achieve a desired characteristic has been proved in the past, especially when the final result was determined by unrelated parameters.[10] Therefore, the method is well suited for analyzing complex sets of process parameters such as those in the ink-jet printing process.

In the present case, the quality of inkjet-printed silver layers will be influenced by factors such as the proportion of water added to the ink defined by the water/ink ratio, the opening time of the nozzle, the jetting pressure and the spacing between ink droplets as reflected by the drop density (i.e. the number of drops per mm). For each of these four control factors, three levels are chosen as shown in Table I. The levels were chosen to ensure the ink printability. For example, a significant thinning of the ink was not feasible as the high water content tended to deform the paper due to water absorption. An $L_9(3^4)$ orthogonal array is employed to study the system response to the control factors. This results in a series of nine experiments as tabulated in Table II.

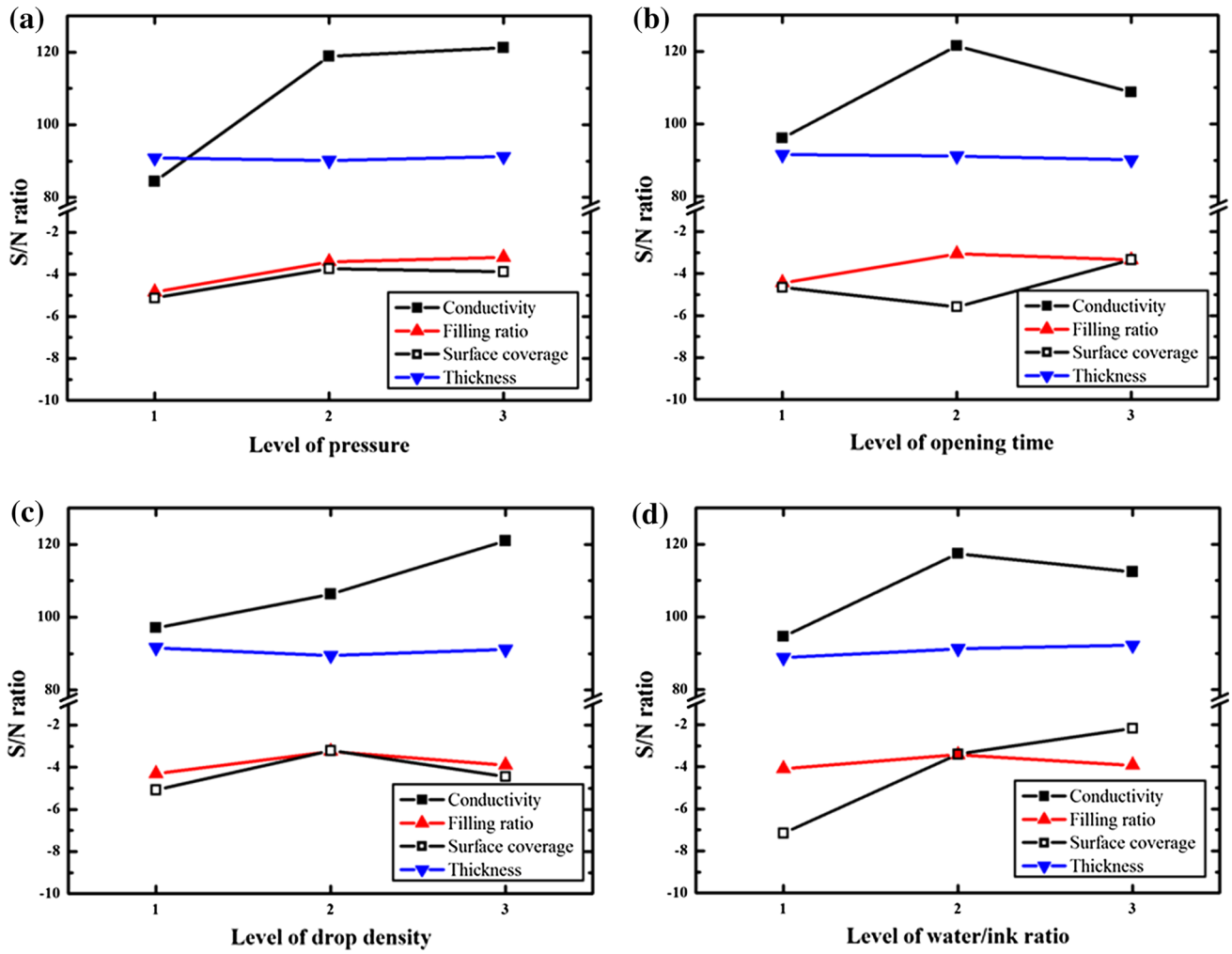

Fig. 9. The effect of: (a) pressure; (b) opening time; (c) drop density; (d) water/ink ratio on the conductivity, filling ratio, surface coverage and layer thickness for the silver tracks printed using ink-jet printing.

The effect of each experimental factor on the conductivity, filling ratio, surface coverage and the thickness of the printed layers is examined by calculating an appropriate signal-to-noise ratio S/N that is defined as the ratio of the signal power (the mean) to noise power corrupting the signal (the standard deviation).[10] In this work, we are looking to optimize the process to provide highest conductivity (as a function of filling ratios and surface coverage) and thinner layers. Therefore, the larger-the-better ratio (LB) and smaller-the-better (SB) ratio, respectively, are used. These are defined as:

$$S/N_{\mathrm{L}} = -10\log\left(\frac{1}{n}\sum_{i=1}^{n}\frac{1}{y_i^2}\right)\ (\mathrm{LB}), \qquad (2)$$

$$S/N_{S} = -10\log\left(\frac{1}{n}\sum_{i=1}^{n}y_i^2\right)\ (\mathrm{SB}). \qquad (3)$$

To optimize a process using the Taguchi method, one attempts to maximize the appropriate signal-to-noise ratio as defined above. Control factors which have the greatest impact on the S/N ratio can be considered to be the most important. The average S/N ratio for each control factor and level can be calculated to examine how the S/N ratio varies.[10]

As used, the Taguchi approach allowed us to determine and optimize the contribution of water/ink ratio, the opening time of the nozzle, the jetting pressure and the spacing between ink droplets as reflected by the drop density. The inner array and the response of the conductivity used in the Taguchi approach are presented in Tables III and IV, respectively. Analyzing the data in Table IIIa–c, one can conclude that a linear dependence between the measured conductivity and the estimated filling ratios and surface coverage cannot be established. The results in Table IV suggest that the least influential factor for the conductivity is the ink thinning (as reflected by the water/ink ratio), while

Table V. Summary of the response table for each parameter

	Water/ink ratio	Pressure	Opening time	Drop density
Conductivity (LB)	4	1	2	3
Filling ratio (LB)	4	1	2	3
Coverage (LB)	1	4	2	3
Thickness (SB)	1	4	3	2

The conductivity and filling ratio have similar influences suggesting the direct relationship between them.

the strongest influence is exerted by the pressure, followed at equal distance by the opening time and drop density.

The increase of the processing pressure led to an initial increase in *S*/*N* ratio followed by saturation to a level where maximum compactness was already reached (Fig. 9a). For opening time (Fig. 9b), the second level seems to be the optimal with a decrease in the *S*/*N* ratio observed afterwards, probably due to the extended spreading of the resulting bigger droplets and emerging of secondary factors such as paper substrate non-uniformities. An increase in drop density led to the expected linear increase in the conductivity (Fig. 9c). One might expect this, as the higher the density the longer the compaction pressure within the coalescing drops was sustained leading to better connectivity between the silver flakes and, therefore, a higher conductivity. The data summarized in Tables IVa–d and V clearly determines the pressure as the most important factor for the conductivity and the filling ratio of the deposited tracks, reflecting the role of the compacting pressure exercised by the landing drops. The least influential factor was found to be the ink thinning described by the water/ink ratio (Fig. 9d) and ranked 4 in Table IVa, b. A similar effect was observed for the doctor-blading (Figs. 4a, c, 5a, c) where the surface coverage and filling ratio remained similar after thinning (Fig. 6). Water/ink ratio appeared to be the most influential factor for the surface coverage and the thickness as it was strongly affecting the ink rheology and consequently the spreading characteristics of the drops.

CONCLUSIONS

In this study, we have demonstrated that conductive silver layers can be successfully deposited onto paper substrates using ink-jet printing at room temperature without a further sintering process. The presented results were obtained using specially formulated aqueous-based ink containing micron-sized silver flakes with narrow size distribution. The results indicate that ink-jet printing is uniquely positioned among several other printing and coating methods for the deposition of this type of ink, leading to the formation of highly conductive percolated material. It was found that there was no linear relationship between the measured conductivity and the estimated filling ratio and surface coverage. This suggests that the variation of the impact pressure of the drops resulted in a complex change of the flakes compaction mechanism. These findings open interesting avenues for further investigation of the fluid dynamics associated with ink-jet deposition technology, in which drops may vary in size from the pl to the nl range depending on the ink-jet printing technology used and the requirements for the ink formulation. Understanding the deposition mechanisms can accelerate the development of paper-based electronics.

ACKNOWLEDGEMENTS

The authors acknowledge the support under the BERNAL (University of Limerick) and TEMPRI projects.

REFERENCES

1. S.M. Bidoki, D.M. Lewis, M. Clark, A. Vakorov, P.A. Millner, and D. McGorman, *J. Micromech. Microeng.* 17, 967 (2007).
2. G. Zheng, Y. Cui, E. Karabulut, L. Wågberg, H. Zhu, and L. Hu, *MRS Bull.* 38, 320 (2013).
3. W. Songping, *J. Mater. Sci* 18, 447 (2007).
4. F.C. Krebs, *Sol. Energy Mater. Sol. Cells* 93, 394 (2009).
5. A.I.Y. Tok, F.Y.C. Boey, and M.K.A. Khor, *J. Mater. Eng. Perform.* 8, 469 (1999).
6. L. Hu, J.W. Choi, Y. Yang, S. Jeong, F. La Mantia, L.F. Cui, Y. Cui, and C.M. Lieber, *Proc. Natl. Acad. Sci. USA* 106, 21490 (2009).
7. C. Bois, A. Blayo, D. Chaussy, R. Vincent, A.G. Mercier, and C. Nayoze, *Fuel Cells* 12, 199 (2012).
8. B. Havlínová, V. Cicák, V. Brezová, and Ľ. Horňáková, *J. Mater. Sci.* 34, 2081 (1999).
9. H. Andersson, A. Manuilskiy, C. Lidenmark, J. Gao, T. Ohlund, S. Forsberg, J. Ortegren, W. Schmidt, and H.E. Nilsson, *Nanotechnology* 24, 455203 (2013).
10. H.S. Chen, R.V. Kumar, and B.A. Glowacki, *J. Sol–Gel. Sci. Technol.* 51, 102 (2009).
11. P.J. Smith, D.Y. Shin, J.E. Stringer, B. Derby, and N. Reis, *J. Mater. Sci.* 41, 4153 (2006).
12. A. Kamyshny, J. Steinke, and S. Magdassi, *Open Appl. Phys. J.* 4, 19 (2011).
13. I. van Driessche, J. Feys, S.C. Hopkins, P. Lommens, X. Granados, B.A. Glowacki, S. Ricart, B. Holzapfel, M. Vilardell, A. Kirchner, and M. Baecker, *Supercond. Sci. Technol.* 25, 065017 (2012).
14. http://www.Tempri.eu.
15. M. Toivakka, D. Eklund, and D.W. Bousfield, *Proceedings of the Technical Association of the Pulp and Paper Industry's Coating Conference*, p. 403 (1992).
16. T.K. Sen and K.C. Khilar, *Adv. Colloid Interface Sci.* 119, 71 (2006).
17. L. Yang, *Nord. Pulp Pap. Res. J.* 28, 94 (2013).

18. I. Iliopoulos and L.E. Scriven, *Phys. Fluids* 17, 127101 (2005).
19. F. Olsson and P. Isaksson, *Nord. Pulp Pap. Res. J.* 10, 234 (1995).
20. J.C. Husband and A.G. Hiorns, *6th European Coating Symposium Conference Proceedings, University of Bradford*, 7th–9th September 2005, UK.
21. D.W. Bousfield, *Rheol. Rev.* 2, 47 (2008).
22. J. Stringer and B. Derby, *Inkjet Technology for Digital Fabrication*, ed. I.M. Hutchings and G.D. Martin (Sussex: Wiley, 2013), p. 113.
23. C. Wang, S.C. Hopkins, R.I. Tomov, R. Vasant Kumar, and B.A. Glowacki, *J. Eur. Ceram. Soc.* 32, 2317 (2012).
24. M. Arin, P. Lommens, S.C. Hopkins, G. Pollefeyt, J. van der Eycken, S. Ricart, X. Granados, B.A. Glowacki, and I. van Driessche, *Nanotechnology* 23, 165603 (2012).